KfK 3582
September 1983

Neutron Capture in s-Wave Resonances of ^{64}Ni

K. Wisshak, F. Käppeler, R. L. Macklin, G. Reffo, F. Fabbri
Institut für Kernphysik

Kernforschungszentrum Karlsruhe

KERNFORSCHUNGSZENTRUM KARLSRUHE
Institut für Kernphysik

KfK 3582

NEUTRON CAPTURE IN s-WAVE RESONANCES OF ^{64}Ni

K. Wisshak, F. Käppeler,
R.L. Macklin[+],
G. Reffo[++], and F. Fabbri[++]

Kernforschungszentrum Karlsruhe GmbH, Karlsruhe

[+] Oak Ridge National Laboratory

[++] E.N.E.A. Bologna

Kernforschungszentrum Karlsruhe GmbH
ISSN 0303-4003

ABSTRACT

The neutron capture widths of the s-wave resonances at 13.9 and 33.8 keV in ^{64}Ni have been determined using a setup with extremely low neutron sensitivity completely different from all previous experiments on this isotope. This feature is important because these resonances exhibit a very large scattering to capture ratio. A pulsed 3-MV Van de Graaff accelerator and a kinematically collimated neutron beam, produced via the ^{7}Li(p,n) reaction, was used in the experiments. Capture gamma-rays were observed by three Moxon-Rae detectors with graphite-, bismuth-graphite-, and bismuth-converter, respectively. The samples were positioned at a neutron flight path of only 6-8 cm. Thus events due to capture of resonance scattered neutrons in the detectors or in surrounding materials are completely discriminated by their additional time of flight. The short flight path and the high neutron flux at the sample position allowed for a signal to background ratio of $\sim$ 1 even for the broad resonance at 33.8 keV. The data obtained with the individual detectors were corrected for the efficiency of the different converter materials. For that purpose, detailed theoretical calculations of the capture gamma-ray spectra of the measured isotope and of gold, which was used as a standard, were performed. The final radiative widths are Γ_γ(13.9 keV) = 1.01 $\pm$ 0.07 eV and Γ_γ(33.8 keV) = 1.16 $\pm$ 0.08 eV, considerably smaller than the rough estimates obtained in previous work.

ZUSAMMENFASSUNG

Neutroneneinfang in s-Wellen Resonanzen von ^{64}Ni.

Die Neutroneneinfangbreiten der s-Wellen Resonanzen in ^{64}Ni bei 13.9 und 33.8 keV wurden mit einer Meßanordnung bestimmt, die extrem unempfindlich gegen gestreute Neutronen ist und sich in diesem Punkt von den bisher für dieses Isotop verwendeten Methoden unterscheidet. Diese Eigenschaft ist deshalb wichtig, weil die untersuchten Resonanzen ein besonders großes Verhältnis von Streuung zu Einfang aufweisen. Mit einem gepulsten 3 MV Van de Graaff Beschleuniger wurde ein kinematisch kollimierter Neutronenstrahl über die ^{7}Li(p,n) Reaktion erzeugt. Die Gammaquanten des Neutroneneinfangs wurden mit drei verschiedenen Moxon-Rae-Detektoren gemessen, die mit einem Graphit-, Wismut-Graphit- bzw. einem Wismut-Konverter ausgerüstet waren. Die Proben waren unter einem Flugweg von nur 6-8 cm aufgestellt. Auf diese Weise wurden Ereignisse, die vom Einfang gestreuter Neutronen im Detektor oder dem umgebenden Material herrühren, vollständig über die zusätzliche Flugzeit diskriminiert. Durch den kurzen Flugweg und den hohen Fluß am Ort der Probe wurde selbst für die sehr breite Resonanz bei 33.8 keV ein Signal-zu-Untergrund-Verhältnis von $\sim$ 1 erreicht.

Die mit verschiedenen Detektoren gemessenen Daten wurden auf die unterschiedliche Ansprechwahrscheinlichkeit der einzelnen Konvertermaterialien korrigiert. Dazu wurden umfangreiche theoretische Rechnungen durchgeführt, um die Einfang-Gammaspektren von ^{64}Ni und des Gold-Standards zu bestimmen. Die Ergebnisse Γ_γ(13.9 keV) = 1.01 $\pm$ 0.07 eV und Γ_γ(33.8 keV) = 1.16 $\pm$ 0.08 eV sind erheblich niedriger als die groben Abschätzungen bisheriger Experimente.

I. INTRODUCTION

The exact determination of the capture widths of broad s-wave resonances in structural materials proved to be a difficult and important task for the characterization of these isotopes. As pointed out in Ref. 1 at the example of ^{56}Fe and ^{58,60}Ni a single s-wave resonance can contribute up to 40 % to the isotopic neutron capture cross section averaged over a fast reactor spectrum. The same holds for the average over a Maxwellian velocity distribution, which is of importance for nuclear astrophysics[2].

Due to the correction for neutron sensitivity the accuracy obtained in LINAC experiments is presently limited to ∿ 30 % for s-wave resonances with $\Gamma_n/\Gamma_\gamma \sim 1000$ (Ref. 3). Recent efforts to reduce the neutron sensitivity by using a low mass setup yielded preliminary values with an accuracy of ∿ 15 % (Ref. 4). Uncertainties of the same order were already obtained in Van de Graaff measurements with a liquid scintillator tank about fifteen years ago (Ref. 5). These large uncertainties, however, do not meet the WRENDA[6] requests for capture cross sections of structural materials.

A few years ago, an experimental method proposed by Macklin et al.[7] was reactivated and optimized (Ref. 8,9). It uses a Van de Graaff accelerator and kinematically collimated neutrons produced in (p,n) reactions on light nuclei. It allows the use of very short flight paths and events due to capture of scattered neutrons are completely eliminated by their additional time of flight (TOF), as the distance from sample to detector is larger than the primary flight path. In Ref. 1 we published data for Γ_γ of s-wave resonances with $\Gamma_n/\Gamma_\gamma \sim 1000$ in ^{56}Fe and ^{58,60}Ni. The overall systematic and statistical accuracy is 5 - 6 %.

The potential of this experimental method should allow to determine the capture widths of resonances with Γ_n/Γ_γ ratios that are even one order in magnitude larger. For such resonances accurate data can hardly be obtained at a LINAC. But in turn, accurate capture widths of such resonances can be used to check and to improve the neutron sensitivity correction of LINAC experiments. This might help to clarify existing discrepancies

for resonances with $\Gamma_n/\Gamma_\gamma \sim 1000$ as discussed above.

In the present experiment we measured the capture widths of two s-wave resonances in ^{64}Ni at 13.9 and 33.8 keV. The final results showed that they have Γ_n/Γ_γ ratios of 2800 and 7700, respectively. Due to their large neutron widths (8.9 keV for the resonance at 33.8 keV) these resonances are spread over many TOF channels in an actual experiment and, therefore, it is very hard to obtain a reasonable signal to background ratio. With the very short flight path of 6 cm and with an optimization for further background reduction our setup allowed to detect the 33.8 keV resonance with a signal to background ratio of one in spite of its small peak cross section of only 10 mb. Thus, an overall statistical and systematic uncertainty of 7 % was obtained even for this extreme case.

II. EXPERIMENTS

The experimental method as well as the data evaluation and the systematic uncertainties have been discussed in detail in Refs. 1,8. Therefore, only the essential features of the present work are outlined here emphasizing the achieved improvements.

The measurements were performed at the Karlsruhe 3-MV pulsed Van de Graaff accelerator. A kinematically collimated neutron beam is produced via the ^{7}Li(p,n) reaction by adjusting the proton energy just above the reaction threshold.

In this case no further collimation is required and the samples can be placed at a flight path as short as 6 - 8 cm. The capture detectors are arranged at backward angles completely outside the neutron cone. The distance from the sample to each detector is $\sim$ 16 cm. Data were taken simultaneously from three Moxon-Rae detectors with graphite, bismuth-graphite and pure bismuth converter, respectively. Two ^{6}Li-glass detectors are used to ensure that all samples are irradiated by the same neutron fluence. A TOF-spectrum is recorded from a transmission

detector located at 0° with respect to the beam axis and a spectrum is taken from a neutron monitor at 20°.

The capture cross section of gold was used as a standard. In addition, data were taken from an empty position in the sample changer frame for background determination. The important parameters of the individual samples are compiled in Table I. While the first run was made with a gold sample of 0.4 mm thickness all furter data were taken with a 0.2 mm thick gold sample in order to reduce the corrections for multiple scattering and gamma-ray self-absorption. All samples were squares, 26 x 26 mm, to match the shape of the ^{64}Ni sample.

The samples were fixed in the sample changer frame by 0.1 mm thick steel wires (15 cm from the sample). Thus, the material closest to the sample where resonance scattered neutrons may be captured is the neutron target itself. The flight paths were measured relative to a stainless steel standard by an eddy current device which was calibrated for each material separately.

Due to the very low peak cross section of the resonance at 33.8 keV the statistical uncertainty contributes significantly to the total accuracy, in contrast to previous measurements. Therefore, the same time-to-pulse height converter was used for all three Moxon-Rae detectors and the individual spectra were separated afterwards by a mixer router unit connected to the ADC. This allowed to add the spectra of all detectors easily and to analyse also the summed spectra.

First test measurements proved that the rough estimates $\Gamma_\gamma \sim 2 - 3$ eV for the resonance at 33.8 keV reported in Ref. (10,11) were significantly too large. The signal to background ratio using the setup of Ref. 1 and a flight path of 90 mm was 1:10 only, indicating a value $\Gamma_\gamma \sim 1$ eV. In order to improve the sensitivity, the experiment was modified in the following points:

a) The accelerator frequency was reduced from 2.5 MHz to 1 MHz. In this way the time interval in which the effect is observed remains the same while the time independent background is spread over a 2.5 times larger interval. Thus the signal

to background ratio is improved but at the expense of an increased measuring time as the average beam current is reduced by about the same factor of 2.5.

b) The backing of the neutron target was made from 0.2 mm thick silver instead of 0.5 mm copper used in the beginning. The essential part of the time-dependent background in the region of the 33.8 keV resonance was found to be caused by neutrons which are scattered in the target backing and are then captured in the lead shielding between neutron target and detectors. The use of silver reduced scattering in the target backing significantly.

The spray water cooled tantalum targets described in Refs. 1 and 8 were replaced already in the beginning by a more effective construction described in Ref. 12. The cooling water flows in a closed ring around the target but outside the neutron cone and the heat is removed by lateral conduction. A further advantage of this target is that the flight path changes by less than 0.1 mm for different targets.

The silver target backing was coated with a thin layer of platinum to stop the protons (thus reducing the gamma-ray production rate) and to avoid diffusion of the lithium into the silver.

c) The lead shielding between neutron target and detectors was minimized. A 1 cm thick ring of lead proved to be sufficient to reduce the intensity in the prompt gamma-ray peak (which essentially determines the total counting rate) by a factor of $\sim$ 4 in all detectors.

d) The thickness of the lithium targets was optimized in such a way that the energy loss of the protons is only slightly larger than the energy difference between proton energy and reaction threshold ($\sim$ 6 keV). In this way a "dead layer" of lithium is avoided where no neutrons are produced but which contributes to the gamma-ray production via inelastic proton scattering.

In our previous experiments the target thickness was $\sim$ two times larger because such targets stand a longer irradiation time and offer a slightly higher neutron intensity.

With these improvements the signal to background ratio for the 33.8 keV resonance was improved by about a factor of three, The count rate of all three Moxon-Rae detectors together was $\sim$ 1.5 kHz so that dead time effects were manageable.

As indicated in Table II three runs have been performed with modified experimental conditions concerning flight paths, proton energies and sample thickness. With the longer flight path of 8 cm the various p-wave resonances which are superposed on the s-wave resonance at 33.8 keV are nearly resolved which facilitates a reliable separation between p- and s-wave components. With the shorter flight path of 6 cm the signal to background ratio is significantly better thus allowing for a smaller statistical uncertainty.

In run II we tried to improve the signal to background ratio further by reducing the proton energy as discussed in Ref. 1. But at the position of the 33.8 keV resonance the neutron flux scaled in first approximation as the neutron fluence and therefore no improvement was obtained. At the top of Figs. 1 to 3 the signal to background ratio of the three measurements is demonstrated. These figures show the TOF spectra measured with the ^{64}Ni sample and the corresponding background spectrum determined with the empty position in the sample changer frame. It was shown in Ref. 1 that the signal to background ratio is the same for all three detectors. Therefore, only the summed spectra of all three detectors are displayed.

A broad bump shows up in the TOF spectra between channels 150 - 220 which was not so obvious in our previous work[1,8]. It is due to the so called debunched beam pulse. The Mobley bunching system of our Van de Graaff accelerator is working at a fixed frequency of 10 MHz. Therefore, a small dc component in the primary beam results in a small satellite pulse every 100 nsec after the main pulse. Between these satellites, namely every 50, 150 ns... after the main pulse, the deflecting electric field has opposite polarity and produces a broad debunched pulse with an intensity which is only $\sim 3 \cdot 10^{-5}$ that of the main pulse. But as in the present experiment all other background components have been significantly reduced this small additional background clearly shows up in the spectra. Unfortunately in

run III a temporary instability of the accelerator increased the debunched pulse by a factor of three. This additional background affects only the resonance at 13.9 keV.

III. DATA ANALYSIS

The data analysis has been described in detail in Refs. 1 and 8. Here, we point out where changes have been made and discuss the individual correction factors. For all runs the spectra of the three Moxon-Rae detectors were analyzed separately, but in addition the summed spectra as shown in Figs. 1 to 3 were analyzed, too. Because of the higher statistical accuracy this offered a better determination of the resonance energies and a more reliable separation of p- and s-wave components.

III A Evaluation of the Capture Yield

Because all TOF spectra were measured through a single electronic chain, correction for a time shift of the prompt gamma-ray peak was not required in the present experiment. Due to the improvements of the target construction and the flight path measurement flight path differences were less than 0.2 mm for different targets and less than 0.1 mm for different samples. Therefore, the transformation of the individual data to a common average flight path was also not necessary. The normalization to equal neutron fluence per sample as determined from the spectra measured with the two ^{6}Li monitors was 0.5 % in runs I and III and negligible in run II. The subtraction of time-dependent and constant backgrounds was performed in the same way as described in Ref. 1. The resulting spectra are shown in the lower part of Figs. 1 to 3. As can be seen from these figures there is a strong residual background, the high energy end of which affects the area of the resonance at 13.9 keV. This background is due to neutrons scattered in the sample and captured in the neutron target or in the detectors and the sample changer frame. The figures illustrate that this background is sufficiently distant not to disturb the area of the measured resonances.

At the bottom of e.g.Fig.3 it is shown that this background consists mainly of two components, one centered around channel number 190 the other around channel number 100. These two components are due to neutrons which are scattered in the 33.8 keV resonance and are then captured in the target backing and the detectors as indicated by the times T_2 and T_3. The position of the prompt gamma-ray peak, T_o, marks the origin of the TOF scale, while T_1 corresponds to the high energy end of the 33.8 keV resonance ($\approx$ 45 keV). At time T_2 = 2 x T_1 the first neutrons scattered in the 33.8 keV resonance reach again the target backing. As no other structural material is located closer to the sample T_2 represents the point of time where capture of scattered neutrons can affect the measured TOF spectra. At time T_3 neutrons scattered in the 33.8 keV resonance reach first the detectors or the sample changer frame. According to their larger distance from the sample (15 - 16 cm) the time difference $T_3 - T_1$ is 2.5 times larger than the time difference $T_2 - T_1$, which corresponds to the flight path of 6 cm. As indicated in Figs. 1 to 3 the background due to capture of scattered neutrons was extrapolated using the condition that it is zero at time T_2. This additional background was subtracted from the spectra before the final capture yield was calculated.

The correction for multiple scattering and self-shielding of the gold samples (see Table I) was calculated with the SESH code of Fröhner[13]. The calculation was performed for a disk sample with equal area as the square samples used in the experiment. As the energy dependence in the region from 14 to 34 keV is low a constant average was assumed for this correction. Very good agreement is found between the corrections so obtained and values calculated with the Dresner formula according to Ref.14 (1.035 and 1.019).

The correction for gamma-ray self-absorption in the gold samples given in Table I has been measured recently. The corresponding value for the nickel sample was calculated as described

in Ref. 8. This simple method is supported by the fact that the respective calculations for the gold samples agreed to better than 0.4 % with the measured values.

An independent check for this correction was made using a code of Macklin[15]. We found values of SA = 0.990 and 0.980 for the thin and thick gold sample, and SA = 0.992 for the nickel sample which is in very good agreement with the factors quoted in Table I.

The gold standard cross section for conversion of the experimental ratios to absolute cross sections was taken from ENDF/B-V in the same way as described in Ref. 1.

III B Determination of the Capture Widths

The capture widths of the s-wave resonances were deduced from the capture yield with the FANAC code of Fröhner[16]. The analysis was performed in the same way as described in Refs. 1 and 8. As the peak cross section of the broad s-wave resonance at 33.8 keV is very low even the small contamination of other nickel isotopes in the sample (see Table I) may affect the results. Therefore, the resonances of ^{58,60}Ni and ^{62}Ni were included in the fits as fixed parameters. The resonance parameters of each isotope were normalized by a constant factor to account for the different binding energy.

For separation of s- and p-wave components in the region of the 33.8 keV resonance we used the p-wave resonance parameters of ^{64}Ni as fixed input. The respective values were taken from a preliminary evaluation of Spencer and Macklin[17]. In order to obtain optimal fits the p-wave resonance parameters were normalized by a common factor. This factor was determined by fitting the strong p-wave resonance at 31.9 keV. It accounts for the possibility that the detector efficiency depends on the capture gamma-ray spectrum of the p-waves and/or for a possible systematic difference of $\sim$ 10 % between the present measurement and the data of Macklin and Spencer.

The ^{64}Ni parameters for the FANAC fits are compiled in Table III. The parameters for ^{58,60}Ni were taken from our work on these isotopes[1], while the data for ^{62}Ni were adopted from Ref. 10. As the whole energy range of the present experiment was fitted simultaneously and as only 50 resonances can be handled by the FANAC code, weak resonances of impurity isotopes had to be neglected in the fits.

As in Ref. 1 the evaluation was repeated assuming Γ_n as a free and also as a fixed parameter. The values for Γ_n were taken from Ref. 18. The final fits are shown in Fig. 4 for the evaluation with fixed Γ_n. The experimental data represent the summed capture yields of all detectors. These data are not yet corrected for the deviations of the detector efficiency from the ideal linear increase with gamma-ray energy which will be described below. Dashed and dotted lines indicate the capture yield of the isotopic impurities and the s-wave resonance at 33.8 keV.

III C Correction for Detector Efficiency

This correction was calculated in the same way as described for ^{56}Fe and ^{58,60}Ni in Ref. 1. Capture gamma-ray spectra for s-, p- and d-wave resonances were calculated in the framework of the statistical model as described in Sec. VII. The shape of the gamma-ray efficiency of the individual converter materials was taken from literature (Ref. 1). Both informations together allow to calculate a correction factor K by which the results for Γ_γ, as obtained with the individual detectors, have to be multiplied. The final correction factors K are compiled in Table IV.

For given orbital angular momentum the results for K differ by less than 0.5 % for the two possible spin states. Therefore only average values for p- and d-waves are given. The data as evaluated from the summed spectra of all three detectors were corrected by the K factor given in the last column of Table IV (which is the mean of the three values for the individual converter materials). This simplified procedure is applicable as the correction factors are only of the order of 5% and as the counting rate in the individual detectors is about the same for the measured resonances.

IV RESULTS

The parameters for the two s-wave resonances in ^{64}Ni at 13.9 and 33.8 keV, as obtained from the FANAC fits, are compiled in Table V. These values are not yet corrected for the different efficiency of the individual detectors. The results from the two different evaluations, taking Γ_n as free or fixed parameter, are quoted separately. The statistical uncertainties which are calculated by the FANAC code are given in brackets. The code multiplies the uncertainty deduced from the error bars of the individual points by the so called error adjustment factor χ. This factor is calculated as the square root of χ^2 obtained in the fit, divided by the number of data points minus number of free parameters. Thus, the uncertainty is increased if the fit is not able to reproduce the data points completely. As can be seen from the tables, optimuum values $\chi \sim 1$ were obtained in run I only. The higher energy resolution in this run allowed for a better representation of the p-wave resonances. A second reason for the lower χ values in run I is that in this case the background subtraction was obviously optimal. Therefore, the agreement between experimental data and fitted curve is very good even in the region of very low cross sections between 18 and 22 keV as can be seen from Fig. 4. Due to the systematic uncertainty in background subtraction this energy range is not so well described by the fits in runs II and III with the consequence of larger χ values. It has to be emphasized that no attempts were made to adjust the background subtraction in order to improve the fits.

No systematic differences are observed in the results for Γ_γ as obtained in the individual runs. Therefore average values were calculated by weighting the individual results according to their statistical uncertainties. When Γ_n was treated as a free parameter the literature values[10] for Γ_n were reproduced to an accuracy of better than 5 %. One exception are the data measured with the bismuth-graphite converter in run II where strong deviations are found. These can be explained, however, by the poorer statistics of this run. As the neutron widths are so well reproduced only small differences in the results for Γ_γ are ob-

tained in the second analysis with Γ_n as a fixed parameter. Following the arguments given in Ref. 1 we used the mean of both analyses as the final value for Γ_γ.

The binding energies of ^{64}Ni and the gold standard are similar, and therefore only small differences of $\pm$ 5 % result from the slightly different efficiencies of the three converter materials. For completeness we quote in Table VI the normalization factors for the intensity of p-wave resonances as determined for the individual runs. For a given converter they agree to $\pm$ 2 % while again systematic differences of $\pm$ 5 % are observed between the three converter materials.

The results obtained with the correction for detector efficiency are compiled in Table VII. The final values are: Γ_γ = 1.01 $\pm$ 0.07 eV for the resonance at 13.9 keV and Γ_γ = 1.16 $\pm$ 0.08 eV for the resonance at 33.8 keV as evaluated from the summed spectra of all three detectors. These values agree to better than 1 % with the results obtained by averaging the radiative widths as measured with the individual converter materials. In the lowest line of Table VI the normalization factors for p-wave resonances have been multiplied by the respective efficiency correction factor K (see Table IV) in order to remove the component due to detector efficiency. The result indicates, that the present measurement yielded a capture area of the p-wave resonances, which is on the average lower by $\sim$ 10 % than the preliminary values of Spencer and Macklin[17] quoted in Table III.

If we compare the present results to the data of Beer and Spencer[10] one has to keep in mind that these data were not corrected for the neutron sensitivity of the liquid scintillator tank. This correction can be applied according to Ref. 5 yielding Γ_γ = 1.6 eV for both resonances which is still significantly larger than the present values. The difference may be accounted for by the 20 % uncertainty quoted by Beer and Spencer [10] to which an additional uncertainty of the neutron sensitivity correction has to be added. Preliminary results from a measurement performed at Oak Ridge at a 20 m flight path yielded even higher values for these radiative widths[11].

This suggests that the neutron sensitivity corrections were underestimated in both cases.

Finally, the present results yield new values Γ_n/Γ_γ of 2900 and 7740 for the resonances at 13.9 and 33,8 keV, respectively. This means that this ratio is nearly one order of magnitude larger for the resonance at 33.8 keV than for the s-wave resonances in ^{56}Fe and $^{58,60}Ni$ which were investigated in Ref. 1.

V. DISCUSSION OF UNCERTAINTIES

The evaluation of the individual systematic uncertainties is discussed in detail in Refs. 1 and 8. The values quoted in Table VIII have been determined from the summed spectra of all three detectors.

V. A Statistical Uncertainty

The uncertainties given in Table V have been determined in the same way as described in Ref. 1.

V. B Systematic Uncertainties of the Capture Yield

The following systematic uncertainties of the capture yield have been considered.

1.) Flight path transformation: The improved construction of the lithium targets and the use of an eddy current device for the determination of the flight path allowed to reduce the systematic uncertainty for the measured flight path to $\pm$ 0.2 mm. The major part of this uncertainty quoted in Table VIII is due to the uncertainty in solid angle (0.5 % and 0.7 % for flight paths of 8. cm and 6. cm, respectively).

2.) Constant background: This uncertainty is smaller in runs II and III compared to run I due to the better signal to background ratio although, by chance, optimal background subtraction was obtained in run I (see Fig. 4 from 18 to 22 keV).

3.) Background due to capture of scattered neutrons in the lithium target backing. This background affects the resonance at 13.9 keV only and amounts to ∿ 7 % of the observed resonance area (see Figs. 1 to 3). It was assumed that this background could be determined with an uncertainty of ± 30 %.

4.) Multiple scattering in the gold sample and the gold standard cross section. These uncertainties are the same as discussed in Ref. 1. The good agreement between the multiple scattering correction calculated with SESH and with the Dresner formula confirms that the quoted uncertainty is a conservative estimate.

5.) Neutron beam intensity. In the present experiment only three positions in the sample changer frame were used, resulting in a shorter cycle time. In addition, the reduced repetition rate of 1 MHz only allowed for beam currents of 7-10 μAmp. Both conditions together lead to a correction of only 0.5 % for normalization of all spectra to equal neutron fluence. An improved accuracy of 0.3 % could therefore be assigned to this effect compared to Ref. 1.

6.) Gamma-ray self-absorption in the samples.
From the excellent agreement between measured and calculated self absorption corrections, SA, for gold samples of different thickness, an uncertainty of 0.5 % was deduced for the ratio SA (^{64}Ni)/ SA (^{197}Au) which is needed for the analysis. This relatively small uncertainty is confirmed by the independent determination of SA using Macklin's code.

V.C Systematic Uncertainties for the Calculations with the FANAC Code.

1.) Systematic uncertainty of the FANAC calculation:
As in Refs. 1 and 8 an uncertainty of 2 % was assumed to account for the uncertainty of fixed parameters like strength functions, nuclear radii, etc. and the multiple scattering correction.

2.) Energy scale. As can be seen from Table V the resonance energies could be determined with uncertainties of 1 % at 13.9 keV and 2.5 % at 33.8 keV. This uncertainty propagates linearly into the results for the resonance areas.

3.) Subtraction of p-wave resonances. The values quoted in Table VI indicate that the normalization factor for the p-component could consistently be determined from a fit to the strong resonance at 31.9 keV with an accuracy of $\pm$ 1 %. In addition, we assumed that the ratio of the resonance area of the p-wave resonance at 31.9 keV and the sum of all other resonances which are superposed on the s-wave resonance at 33.8 keV is correct to within 2 %. This assumption is justified by the statistical accuracy of Linac experiments (see e.g. Ref. 3). In this way we end up with an uncertainty of 1.7 % for this effect.

4.) Isotopic impurities. The contribution of isotopic impurities to the capture yield in the region of the s-wave resonances is 5.5 % at 13.9 keV and 9.6 % at 33.8 keV. We assumed an accuracy of 10 % for the isotopic correction at 13.9 keV as most of it is due to s-wave resonances in ^{58,60}Ni which were determined with high accuracy in Ref. 1. At 33.8 keV isotopic impurities are dominated by p-wave resonances in ^{58}Ni for which no consistent data are available until now. Therefore we assumed an uncertainty of 20 % for this correction.

V.D Systematic Uncertainty of the Efficiency Correction

For the uncertainty of this correction the same arguments hold as discussed in detail in Ref. 1 for s-wave resonances in ^{56}Fe and ^{68,60}Ni. In the present case no experimental data for the partial capture widths to the ground state or the first excited states exist. Therefore we assumed an uncertainty of $\pm$ 80 % for the intensity of the bin with highest energy in the capture gamma-ray spectrum. This uncertainty is caused by Porter Thomas fluctuations as this bin contains only gamma transitions to the ground state and to the first two excited states in ^{65}Ni (see Ref. 1).

It results in an uncertainty of 1.2 % for the correction factor K. An additional uncertainty of 0.5 % was assumed for the shape of the remaining energy bins. The uncertainty due to the shape of the gamma-ray efficiency is 2.0 % in the present case, and additional 0.5 % account for the uncertainty of the gold spectrum. Thus the total uncertainty of the efficiency correction is 2.4 %.

VI. MAXWELLIAN AVERAGE CROSS SECTIONS

For applications in nuclear astrophysics the Maxwellian average cross section of ^{64}Ni is of importance[18]. According to the definition outlined in Ref. 8, Maxwellian average capture cross sections are quoted for several thermal energies in Table IX. These values were calculated using the present results for the s-wave resonances at 13.9 and 33.8 keV and the preliminary values of Spencer and Macklin [17] for all other resonances in ^{64}Ni. The last column demonstrates that the resonance parameters of the two s-wave resonances contribute about 60 % of the Maxwellian averages.

VII. CALCULATIONS OF CAPTURE GAMMA-RAY SPECTRA

The capture gamma-ray spectra of s-, p-, and d-wave resonances in ^{64}Ni were calculated in the framework of the statistical model using the same method as described in Ref. 1. In the calculations M1 contributions were included as they were found to be of importance especially for p-wave resonances. E2 transitions were treated in the same way as described in Ref. 19. We renounced to consider valence contributions in the present case as they were found to be much smaller than the spectrum uncertainty due to Porter Thomas fluctuations.

VII. A Level scheme

The level scheme of the compound nucleus ^{65}Ni has been adopted (with some modifications) from Lederer and Shirley[20] and is given in Table X. Uncertain spin and parity assignments are put in brackets. The obvious dominance of negative parity levels means that the gamma decay of p-wave resonances is governed by M1 transitions. As no experimental branching ratios for the decay of the discrete levels are available, these have been estimated from Weisskopf single particle transitions assuming only E1 and M1 transitions.

The cumulative number of discrete levels known from experiments is plotted in Fig. 5. It indicates a possible loss of levels between 0.7 and 1.0 MeV and a considerable loss of levels above 1.6 MeV. In order to assess the necessary, complete information for the intended gamma-ray decay calculation the isobaric level schemes have been considered. For example, the dashed line in Fig. 5 describes N(E) for ^{65}Zn which confirms the adopted trend for ^{65}Ni as given by the solid curve. Based on these arguments we have introduced four hypothetical levels in ^{65}Ni which are marked by asterisks in Table X. The respective parities were assigned again in analogy to the situation in the A = 65 isobars of Zn, Ga, Cu which all exhibit a clear preference of negative parity states below 2 MeV, and the spins were chosen according to the spin distribution of the levels in ^{65}Ni (see insert of Fig. 5).

VII.B Level density

From the fit of the composite Gilbert Cameron formula to the experimental data we found that in the considered energy interval only the component ρ_1 is of relevance. Thus, the discrete levels and the resonance spacings could be fitted with the following parameters: U_x = 5.98 MeV and T = .984 MeV. For the spin cut-off factor a value σ^2 = 3.6 was used.

VII.C Average Resonance Parameters

The resonance scheme in the neutron energy range up to 583 keV as compiled by Mughabghab [21] was statistically analyzed in terms of the truncated Porter Thomas distribution and by the maximum likelihood method yielding $23 < D_{OBS} < 29$ keV. This result is somewhat larger than quoted by Mughabghab [21] where $D_{OBS} = 19.9 \pm 3.6$ keV is given. For our calculation $D_{OBS} = 28$ keV was adopted concordant with the level density parameter $a = 9.6\ MeV^{-1}$ resulting from systematics[22]. With these parameters we find the s-wave strength function $S_o = 2.5 \times 10^{-4}$ in good agreement with $S_o = (2.9 \pm 0.8) \times 10^{-4}$ given by Mughabghab [21].

VII.D Radiative Widths

The probability for gamma decay plays an important role in the calculation of capture gamma-ray spectra. A sensitive test of the adopted parametrization is provided by the comparison of calculated and theoretical total radiative widths.

For an estimate of the E1 contribution we assumed a deformation parameter $\beta = 0.25$ which gives - according to the systematics of Reffo [22] - the following parameters of the split giant dipole resonance: $E_1 = 14.86$ meV, $\Gamma_1 = 3.45$ MeV, $\sigma_1 = 60$ mb and $E_2 = 18.43$ MeV, $\Gamma_2 = 5.07$ MeV, $\sigma_2 = 80$ mb.

The M_1 contribution was calculated from the Axel model. In addition we assumed the ratio $\Gamma_\gamma(E1) / \Gamma_\gamma(M1) = 2.4$ following Kopecky [23]. Taking the peak energy of the giant resonance from the relation $E_R = 45\ \bar{A}^{1/3}$ and $\Gamma_R = 5$ MeV as suggested by Kopecky [23] one then obtains the peak cross section $\sigma_R = 7$ mb. The E2 contributions were included in the same way as discussed in Ref. 19. The giant resonance parameters used are: $E = 15.7$ MeV, $\Gamma = 2.35$ MeV, and $\sigma = 7$ mb.

With the above information on the relevant parameters we calculated the radiative widths for s- and p-wave capture as summarized in Table XI. The quoted uncertainties indicate the

tatistical fluctuations. Within these limits we reproduce the experimental results of this work (see Table VII) thus confirming our parametrization.

VII. E Results of the spectra calculations

The calculated capture gamma-ray spectra for s-, p-, and d-wave neutrons are plotted in Fig. 6. The figure shows the relative shape of the spectra normalized to equal integral intensity for s-, p-, and d-waves. For p- and d-waves the average of the calculations for both spin states is given. These spectra were used to calculate the efficiency correction factors K (see Sec. III.C). As already mentioned in Ref. 1 the last bin in the high energy tail of the spectrum exhibits large statistical uncertainties because there only few single transitions are lumped together. The expected standard deviation is

$$\sigma = \sqrt{\frac{2}{\nu} \sum_i \langle \Gamma_i \rangle}$$

with ν being the effective number of degrees of freedom of the lumped distribution $\sum_i \langle \Gamma_i \rangle$. In view of this large uncertainty possible valence contributions are not significant and were therefore not discussed in detail. As was shown recently[24] these uncertainties cannot be reduced by theoretical arguments. In the main part of the spectra statistical fluctuations are greatly reduced and therefore our calculation of an average spectrum is much more reliable.

REFERENCES

1.) K. WISSHAK, F. KÄPPELER, G. REFFO, and F. FABBRI, "Neutron Capture in s-Wave Resonances of ^{56}Fe, ^{58}Ni, and ^{60}Ni", KfK 3516 Kernforschungszentrum Karlsruhe (1983)

2.) P.A. SEEGER, W.A. FOWLER, and D.D. CALYTON, Ap. J. Suppl. 11, 121 (1965)

3.) C.M. PEREY, J.A. HARVEY, R.L. MACKLIN, R. R. WINTERS, and F.G. PEREY, "Neutron Transmission and Capture Measurements and Analysis of ^{60}Ni from 1 to 450 keV", ORNL-5893, ENDF-330 Oak Ridge National Laboratory 1982

4.) F. CORVI, A. BRUSEGAN, R. BUYL, G. ROHR, R. SHELLEY, T. VAN DER VEEN, Proc. Conf. Nuclear Data for Science and Technology, Antwerp 6-10 September 1982, D. Reidel Publishing Company Dordrecht Holland (1983) p. 131

5.) F.H. FRÖHNER, Proc.of a Specialists Meeting on Neutron Data of Structural Materials for Fast Reactors, Geel 5-8 Dec. 1977, Pergamon Press Oxford (1979) p. 138

6.) N.DAYDAY, Ed. "World Request List for Nuclear Data", INDC (SEC) - 78 / URSF International Atomic Energy Agency, Vienna 1981

7.) R.L. MACKLIN, J.H. GIBBONS, and T. INADA, Nucl. Phys. 43, 353 (1963)

8.) K. WISSHAK and F. KÄPPELER, Nucl. Sci. Eng. 77, 58 (1981)

9.) B.J. ALLEN, D.D. COHEN, and F.Z. COMPANY, J. Physics G: Nucl. Phys. 6, 1173 (1980)

10.) H. BEER and R.R. SPENCER, Nucl. Phys. A240, 29 (1975)

11.) R.L. MACKLIN, private communications

12.) K. WISSHAK, J. WICKENHAUSER, F. KÄPPELER, G. REFFO, and F. FABBRI, Nucl. Sci. Eng. 81, 396 (1982)

13.) F.H. FRÖHNER, "SESH - A Fortran IV Code for Calculating the Self-Shielding and Multiple Scattering Effects for Neutron Cross Section Data Interpretation in the Unresolved Resonance Region", GA-8380, Gulf General Atomic (1968)

14.) R.L. MACKLIN, Nucl. Instrum. Methods 26, 213 (1964)

15.) R.L. MACKLIN, unpublished

16.) F. H. FRÖHNER, "FANAC - A Shape Analysis Program for Resonance Parameter Extraction from Neutron Capture Data for Light- and Medium Weight Nuclei", KfK-2145, Kernforschungszentrum Karlsruhe (1977)

17.) R.R. SPENCER and R.L. MACKLIN, private communications 1982

18.) F. KÄPPELER, H. BEER, K. WISSHAK, D.D. CLAYTON, R.L. MACKLIN, and R.A. WARD, Ap. J. 257, 821 (1982)

19.) G. REFFO, F. FABBRI, K. WISSHAK, and F. KÄPPELER, Nucl. Sci.Eng. 83, 401 (1983)

20.) C.M. LEDERER and V.S. SHIRLEY, Tables of Isotopes, 7^{th} ed., John Wiley and Sons, Inc. New York (1978)

21.) S.F. MUGHABGHAB and D.I. GARBER, Neutron Cross Sections, Vol. I, Neutron Resonance Parameters, BNL 325 3^{rd} ed., 1973 Brookhaven National Laboratory, Upton, New York

22.) G. REFFO, in Nuclear Theory for Applications, IAEA-SMR 43, International Atomic Energy Agency Vienna (1980)

23.) J. KOPECKY, Proc. of the Fourth Int. Conf. on Neutron Capture Gamma Ray Spectroscopy, Grenoble France 7-11 September 1981 Conference Series Nr. 62 The Institute of Physics Bristol and London (1982) p. 423

24.) A. MENGONI, G. REFFO, and F. FABBRI
Proc. Conf. Nuclear Data for Science and Technology, Antwerp 6-10 September 1982
D. Reidel Publishing Company Dordrecht Holland 1983, p. 755

Table I Compilation of the Relevant Sample Data

Sample	Chemical Composition	Isotopic Composition (%)	Weight (g)	Thickness (atom/b)	Thickness (mm)	Multiple Scattering in s-Wave Resonance (in % of primary capture events)	Gamma-Ray Self-Absorption SA
^{64}Ni	Metal	0.92 (58) 0.13 (60) 0.05 (61) 0.38 (62) 97.92 (64)	2.176	3.034×10^{-3}	0.46	62 (13.9 keV) 32 (33.8 keV)	0.994
^{197}Au	Metal	natural	5.394 2.804	2.440×10^{-3} 1.268×10^{-1}	0.40 0.20	1.035[a] 1.025[a]	0.984 0.992

Sample size: 26 x 26 mm

[a] Correction for multiple scattering and resonance self-shielding

Table II Important Parameters of the Individual Measurements.

Run	Sample 1	Sample 2	Flight Path (mm)	Neutron Energy Range (keV)	Measuring Time per Sample (h)
I	^{64}Ni	^{197}Au (0.4 mm)	80.4	10 to 60	43.5
II	^{64}Ni	^{197}Au (0.2 mm)	61.2	15 to 55	34.2
III	^{64}Ni	^{197}Au (0.2 mm)	60.1	10 to 60	34.1

Table III Fixed ^{64}Ni Parameters for the FANAC Fits.

s-wave strength function: 2.9×10^{-4}

s-wave radius: 7.5 fm

p-wave radius: 5.4 fm

s-wave resonances:

E (keV)	Γ_n (keV)
13.9	2.9
33.8	8.9

p-wave resonances:

E (keV)	g	Γ_n (eV)	Γ_γ (eV)	$g\frac{\Gamma_n\Gamma_\gamma}{\Gamma}$
25.8	1	3	0.140	0.134
27.4	2	3	0.018	0.035
31.9	1	3	0.739	0.593
39.4	2	1	0.160	0.276
45.8	1	3	0.108	0.104
46.7	2	1	0.064	0.121
60.1	2	3	0.094	0.183
62.7 62.8	1	3	1.140	0.820

Table IV Efficiency Correction Factors K for a Relative Measurement of ^{64}Ni and Gold Using Moxon-Rae Detectors with Different Converter Materials

	Converter Material			
	Graphite	Bismuth-Graphite	Bismuth	Sum of all Detectors
s-Wave	1.040	0.995	0.934	0.990
p-Wave	1.004	0.985	0.957	0.982
d-Wave	1.033	0.984	0.922	0.980

Table V Results for the s-Wave Resonances at 13.9 keV and 33.8 keV in ^{64}Ni but not yet Corrected for Detector Efficiency

Run		Graphite Converter				Bismuth-Graphite Converter				Bismuth Converter				Sum of all Detectors			
		E_n (keV)	Γ_n (keV)	Γ_γ (eV)	χ	E_n (keV)	Γ_n (keV)	Γ_γ (eV)	χ	E_n (keV)	Γ_n (keV)	Γ_γ (eV)	χ	E_n (keV)	Γ_n (keV)	Γ_γ (eV)	χ
Evaluation 1	I	13.66	3.38(15.1)	1.00(10.5)	1.09	13.89	2.83(13.5)	0.99(0.2)	0.92	13.70	2.89(14.7)	1.07(10.5)	1.12	13.75	2.99(8.4)	1.03(5.9)	1.05
Γ_n Free	II	14.01	2.57(24.5)	0.92(15.7)	1.22	14.02	2.78(25.7)	1.02(16.2)	1.24	13.74	2.67(23.9)	1.02(16.4)	1.27	13.89	2.61/14.8)	1.02(10.9)	1.62
Parameter	III	13.96	2.45(17.4)	0.85(11.6)	1.21	14.08	2.32(14.2)	1.01(9.8)	1.07	13.70	3.00(15.3)	1.12(10.5)	1.18	13.90	2.66(11.7)	1.01(7.7)	1.52
Average		13.9	2.78(10.5)	0.92(7.0)		14.0	2.56(9.2)	1.00(6.2)		13.7	2.89(9.7)	1.08(6.7)		13.9	2.81(6.2)	1.02(4.3)	
	I	34.78	8.68(15.6)	1.06(11.3)		34.95	8.33(13.5)	1.15(9.2)		33.96	9.61(15.1)	1.18(11.1)		34.67	8.86(8.2)	1.16(5.7)	
	II	35.37	8.31(21.5)	1.18(14.0)		34.45	3.62(32.)	1.00(13.5)		34.25	6.96(23.9)	1.06(15.5)		34.65	7.36(18.1)	1.15(11.1)	
	III	35.03	9.66(13.0)	1.31(8.6)		35.07	8.84(13.5)	1.24(8.7)		34.43	8.28(14.3)	1.12(9.5)		34.75	8.70(10.5)	1.19(6.8)	
Average		35.01	9.02(9.1)	1.19(6.2)		34.08	6.91(9.6)	1.15(5.7)		34.2	8.38(9.6)	1.13(6.5)		34.7	8.58(6.1)	1.17(4.1)	
Evaluation 2	I		2.9	0.95(7.3)	1.09		2.9	0.99(6.4)	0.90		2.9	1.06(7.5	1.11		2.9	1.02(4.0)	1.05
Γ_n Fixed	II			0.95(12.2)	1.21			0.99(14.4)	1.38			1.03(12.9)	1.26			0.99(9.1)	1.52
Parameter	III			0.89(8.6)	1.20			1.08(6.9)	1.10			1.11(7.8)	1.17			1.03(5.8)	1.51
Average				0.93(5.1)				1.02(4.4)				1.08(5.0				1.02(3.1)	
	I		8.9	1.10(6.7)			8.9	1.20(5.6)			8.9	1.14(6.9)			8.9	1.15(3.7)	
	II			1.19(9.3)				1.18(11.3)				1.16(10.2)				1.18(7.0	
	III			1.24(5.6)				1.25(5.6)				1.12(6.3)				1.19(4.4)	
Average				1.18(3.9				1.22(3.7)				1.14(4.2)				1.16(2.6)	
Mean Value of Both Evaluations		13.9 35.0		0.93(6.1) 1.19(5.1)		14.0 34.1		1.01(5.3) 1.19(4.7)		13.7 34.2		1.08(5.9) 1.14(5.4)		13.9 34.7		1.02(3.7) 1.17(3.4)	

a) The resonance energies are the same for both evaluations.

Table VI Normalization Factors for p-wave Resonances

	Converter - Material			
Run	Graphite	Bismuth-Graphite	Bismuth	Sum of all Detectors
I	0.886	0.930	0.956	0.906
II	0.865	0.920	0.971	0.914
III	0.844	0.910	0.985	0.921
Average	0.865	0.920	0.971	0.914
Corrected for Detector Efficiency	0.868	0.906	0.929	0.897

Table VII Final Results for the Capture Widths of s-Wave Resonances in ^{64}Ni at 13.9 and 33.8 keV.

Resonance Energy (keV)	Converter Material			Sum of all Detectors (eV)	Uncertainty (%)		
	Graphite (eV)	Bismuth-Graphite (eV)	Bismuth (eV)		statis-tical	system-atic	total
13.9	0.97	1.01	1.01	1.01	3.7	5.7	6.8
33.8	1.24	1.18	1.06	1.16	3.4	6.2	7.1

Table VIII Systematic Uncertainties of the Capture Widths of s-Wave Resonances in ^{64}Ni at 13.9 and 33.8 keV (%).

Run	13.9 keV Resonance			33.8 keV Resonance		
	I	II	III	I	II	III
^{64}Ni						
Sample:						
Flight path transformation	0.6	0.8	0.8	0.6	0.8	0.8
Constand Background	3.5	2.7	2.9	3.4	2.3	2.5
Background from scattered neutrons	2.1	2.1	2.1	-	-	-
Gold						
Sample:						
Flight path transformation	0.6	0.8	0.8	0.6	0.8	0.8
Constant background	0.2	0.2	0.2	0.1	0.1	0.1
Multiple scattering	0.7	0.7	0.7	0.7	0.7	0.7
Capture cross section	2.5	2.5	2.5	2.5	2.5	2.5
Neutron beam intensity	0.3	0.3	0.3	0.3	0.3	0.3
Gamma-ray self-absorption	0.5	0.5	0.5	0.5	0.5	0.5
Fanac calculation	2.0	2.0	2.0	2.0	2.0	2.0
Energy scale	1.0	1.0	1.0	2.5	2.5	2.5
Subtraction of p-waves	-	-	-	1.7	1.7	1.7
Isotopic impurities	0.6	0.6	0.6	1.9	1.9	1.9
Detector efficiency	2.3	2.3	2.3	2.3	2.3	2.3
Total systematic uncertainty	5.9	5.6	5.7	6.4	6.0	6.1
Averaged value of all runs		5.7			6.2	

Table IX Maxwellian Average Cross Sections of ^{64}Ni for Various Thermal Energies

Thermal Energy (keV)	$\frac{\langle\sigma v\rangle}{v_T}$ (mb)	
	total	contribution of s-wave resonances at 13.9 and 33.8 keV
2o	13.7	10.1 (73.6 %)
25	11.9	8.1 (68.1 %)
30	10.7 ± 0.9	6.7 (63.0 %)
35	9.8	5.8 (58.5 %)
40	9.2	5.0 (54.5 %)

Table X Adopted Level Scheme for the Compound Nucleus $^{65}Ni^{++}$

Level Number	Energy (MeV)	Spin	Parity	Branching Ratios
1	0.0	2.5	-	- -
2	0.064	0.5	-	(1,100%)
3	0.311	1.5	-	(1, 67%) (2,33%)
4	0.692	1.5	-	(1, 52%) (2,39%) (3, 9%)
5 *	0.850	(2.5)	(-)	(1, 80%) (3,20%)
6	1.01	4.5	+	(1,100%)
7	1.14	(1.5)	(-)	(1, 43%) (2,37%) (3,17%) (4,3%)
8	1.27	(0.5)	(-)	(2, 62%) (3,31%) (4, 7%)
9	1.418	(1.5)	(-)	(1, 39%) (2,34%) (3,19%) (4,5%) (5,3%)
10	1.5	(2.5)	(-)	(1, 57%) (3,29%) (4, 9%) (5,5%)
11	1.6	(0.5)	(-)	(2, 56%) (3,32%) (4,11%) (7,1%)
12 *	1.7	(2.5)	(-)	(1, 52%) (3,28%) (4,11%) (5,7%) (7,2%)
13	1.78	(1.5)	(-)	(1, 34%) (2,31%) (3,20%) (4,8%) (5,5%) (7,2%)
14 *	1.85	(3.5)	(-)	(1, 80%) (5,13%) (6,7%)
1	1.92	2.5	+	(1, 48%) (3,28%) (4,13%) (5,8%) (7,3%)
*	1.97	(1.5)	(-)	(1, 34%) (2,29%) (3,19%) (4,9%) (5,6%) (7,2%) (8,1%)

The J,π characteristics between perentheses were arbitrarily assigned close to the most probable observed values. Underlined gamma-decay characteristics were estimated as described in the text. Levels marked by asterisks are artificially introduced in order to get a better description of the level density (see text).

Table XI Calculated Average E1 and M1 Contributions to the Total Radiative Width for s-, p-, and d-Wave Resonances in ^{64}Ni

l	J^{π}	$\bar{\Gamma}_{\gamma}$ (E1)	ν_{eff}	$\bar{\Gamma}_{\gamma}$ (M1)	ν_{eff}	$\bar{\Gamma}_{\gamma}$ (Total)
0	$1/2^{+}$	790 ± 340	11	60 ± 20	15	850 ± 350
1	$1/2^{-}$	170 ± 60	15	320 ± 150	10	490 ± 150
	$3/2^{-}$	160 ± 60	17	270 ± 100	14	430 ± 100
2	$3/2^{+}$	660 ± 240	15	60 ± 20	16	720 ± 250
	$5/2^{+}$	440 ± 160	15	50 ± 15	18	490 ± 160

FIGURE CAPTIONS

Fig. 1 Experimental TOF spectra measured with the ^{64}Ni sample and with an empty position in the sample changer frame (background) in run I (upper part). The background subtracted spectrum shows the residual background due to capture of scattered neutrons. This component was subtracted in the region of the 13.9 keV resonance as indicated by the histogramm (lower part). Four time marks are given:

T_o: Position of prompt gamma-ray peak, which corresponds to zero point of TOF scale.

T_1: First neutrons are scattered in the 33.8 keV resonance.

$T_2 = 2 \times T_1$: First of these scattered neutrons reach again the neutron target.

T_3: First of these scattered neutrons reach the detectors or the sample changer frame.

These time marks illustrate the TOF discrimination of events due to capture of scattered neutrons.

Fig. 2 TOF spectra of run II in the same representation as Fig. 1

Fig. 3 TOF spectra of run III in the same representation as Fig. 1

Fig. 4 Fanac-fits to the capture yield of ^{64}Ni as obtained in runs I to III. The contribution due to isotopic impurities (dotted line) and due to the s-wave resonance at 33.8 keV (dashed line) are given separately.

Fig. 5 Comparison between the calculated cumulative number of levels (solid line) and known discrete levels for ^{65}Ni and ^{65}Zn (dashed). The energy E_{cut} where the level continuum was supposed to start is marked by an arrow. The theoretical spin distribution and the spin distribution of discrete levels below E_{cut} are given in the insert.

Fig. 6 Calculated capture gamma-ray spectra for s-, p-, and d-wave resonances in ^{64}Ni.

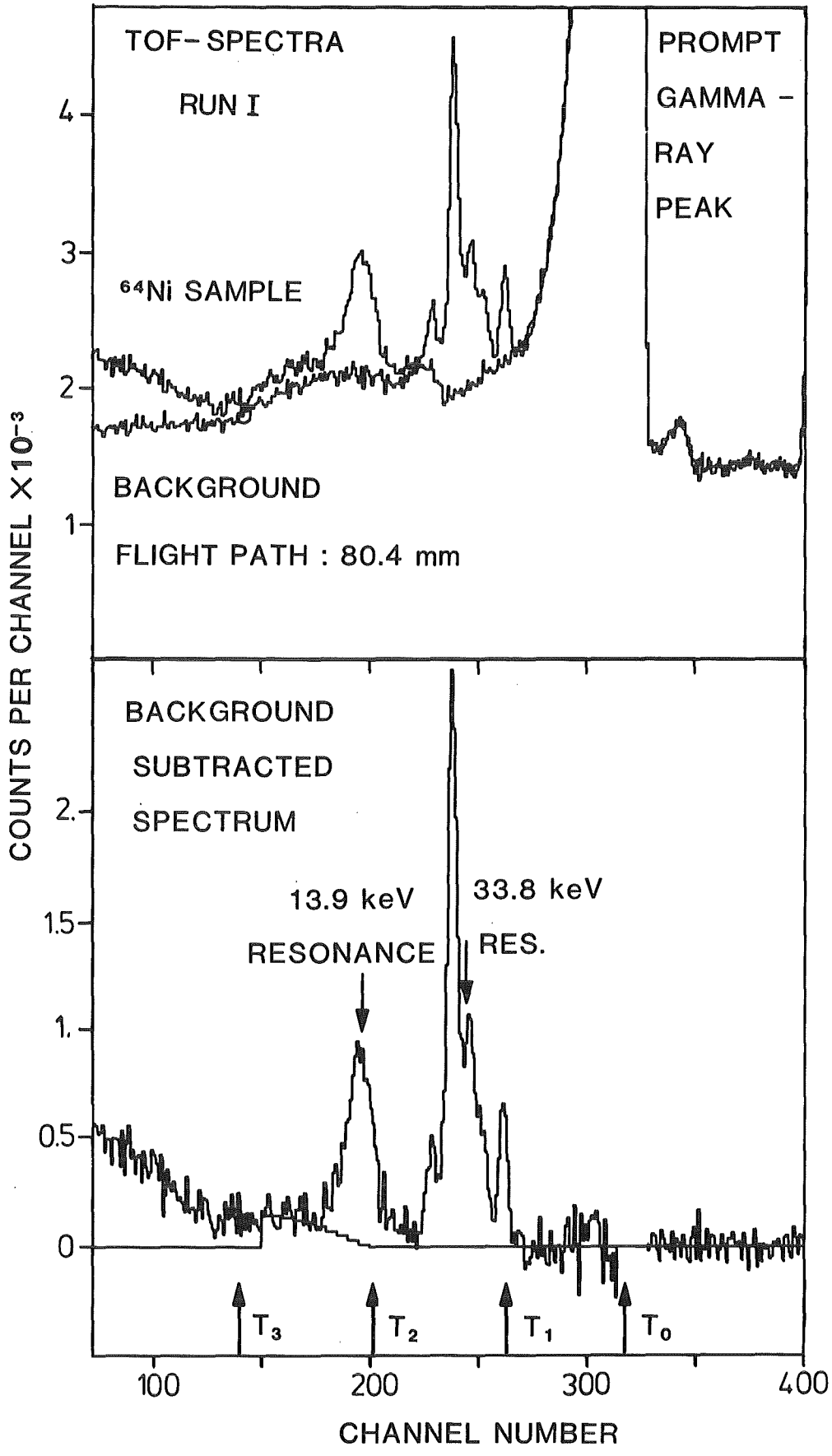
TOF-SPECTRA
RUN I
PROMPT
GAMMA -
RAY
PEAK
64Ni SAMPLE
BACKGROUND
FLIGHT PATH : 80.4 mm
BACKGROUND
SUBTRACTED
SPECTRUM
13.9 keV
RESONANCE
33.8 keV
RES.
T3
T2
T1
T0
COUNTS PER CHANNEL X10-3
CHANNEL NUMBER
4
3
2
1
2.
1.5
1.
0.5
0
100
200
300
400

Fig. 1

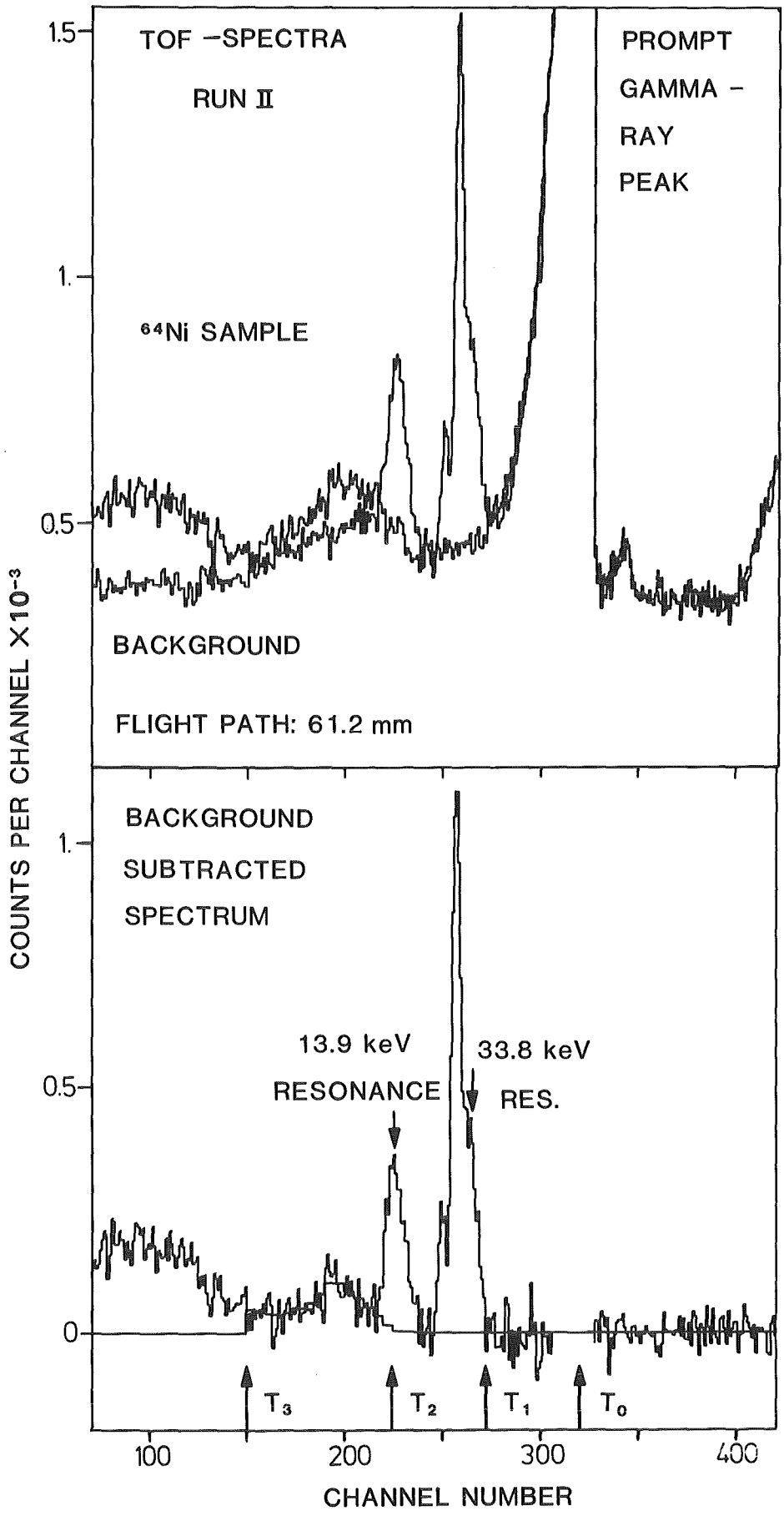
TOF –SPECTRA
RUN II
PROMPT
GAMMA –
RAY
PEAK
64Ni SAMPLE
BACKGROUND
FLIGHT PATH: 61.2 mm
BACKGROUND
SUBTRACTED
SPECTRUM
13.9 keV
RESONANCE
33.8 keV
RES.
T3
T2
T1
T0
COUNTS PER CHANNEL X10-3
CHANNEL NUMBER
1.5
1.
0.5
0
100
200
300
400

Fig. 2

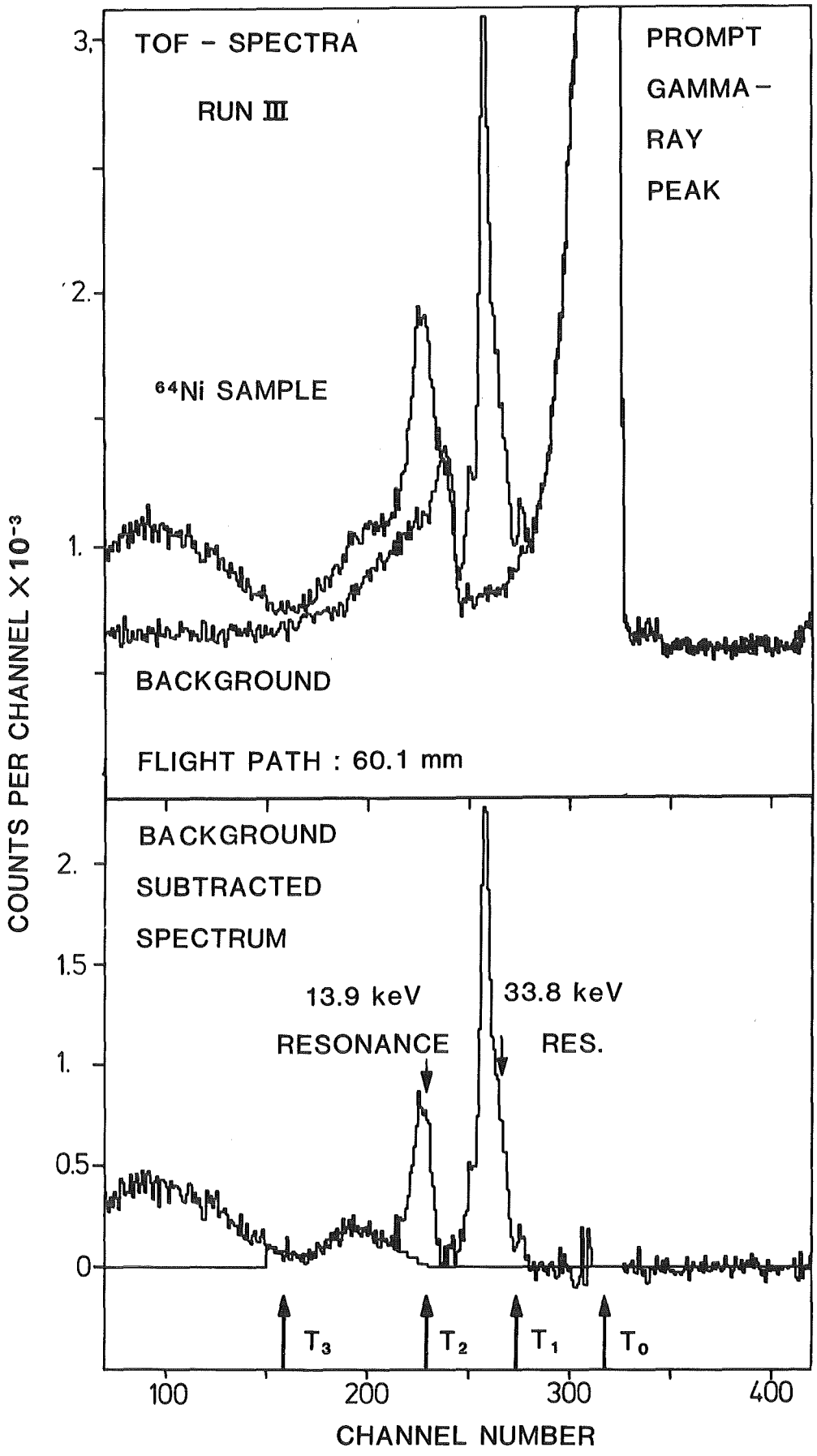
TOF - SPECTRA
RUN III
PROMPT
GAMMA-
RAY
PEAK
64Ni SAMPLE
BACKGROUND
FLIGHT PATH : 60.1 mm
BACKGROUND
SUBTRACTED
SPECTRUM
13.9 keV
RESONANCE
33.8 keV
RES.
T3
T2
T1
T0
COUNTS PER CHANNEL X10-3
CHANNEL NUMBER
3.
2.
1.
0.5
0
100
200
300
400

Fig. 3

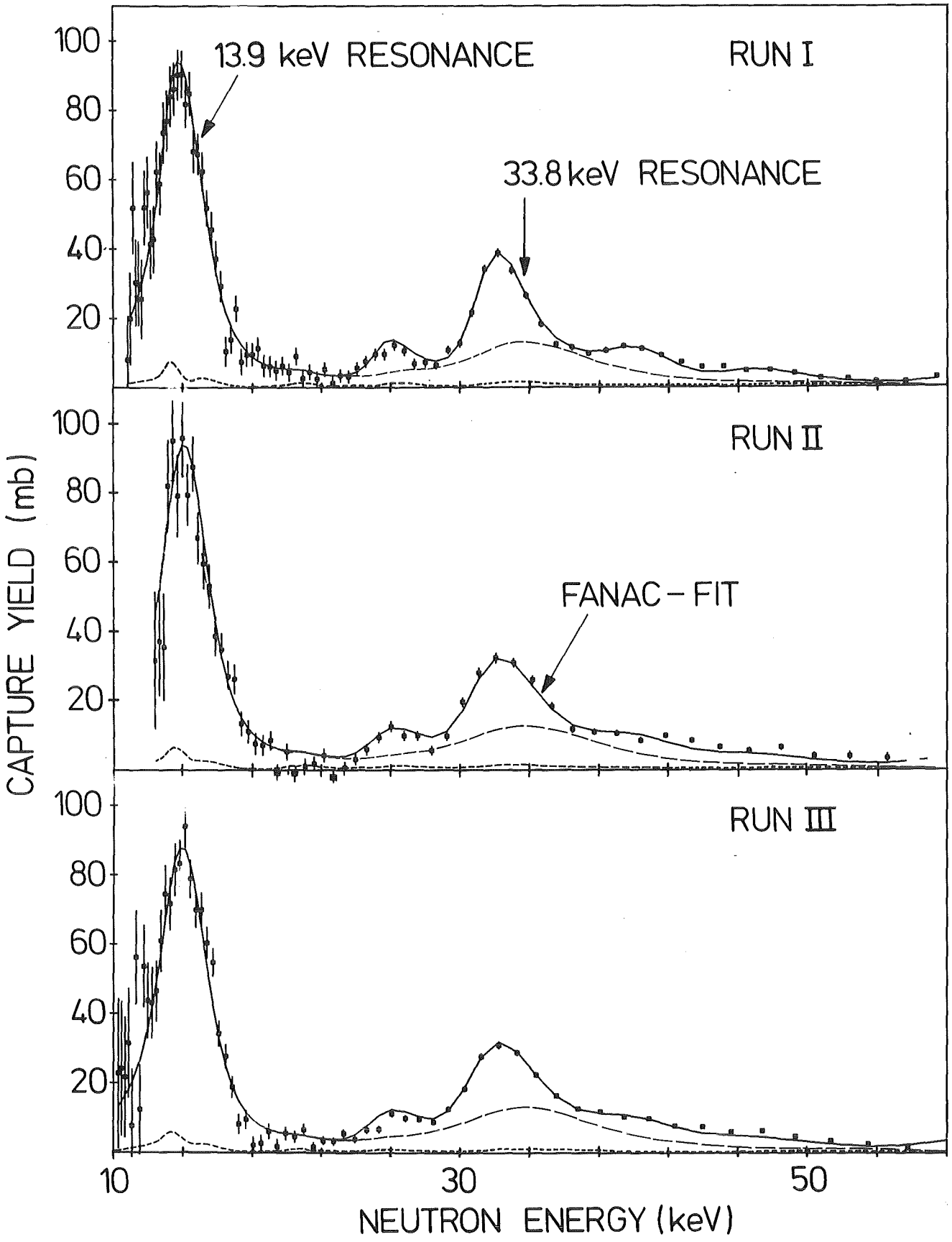
13.9 keV RESONANCE
RUN I
33.8 keV RESONANCE
RUN II
FANAC – FIT
RUN III
CAPTURE YIELD (mb)
NEUTRON ENERGY (keV)
100
80
60
40
20
10
30
50

Fig. 4

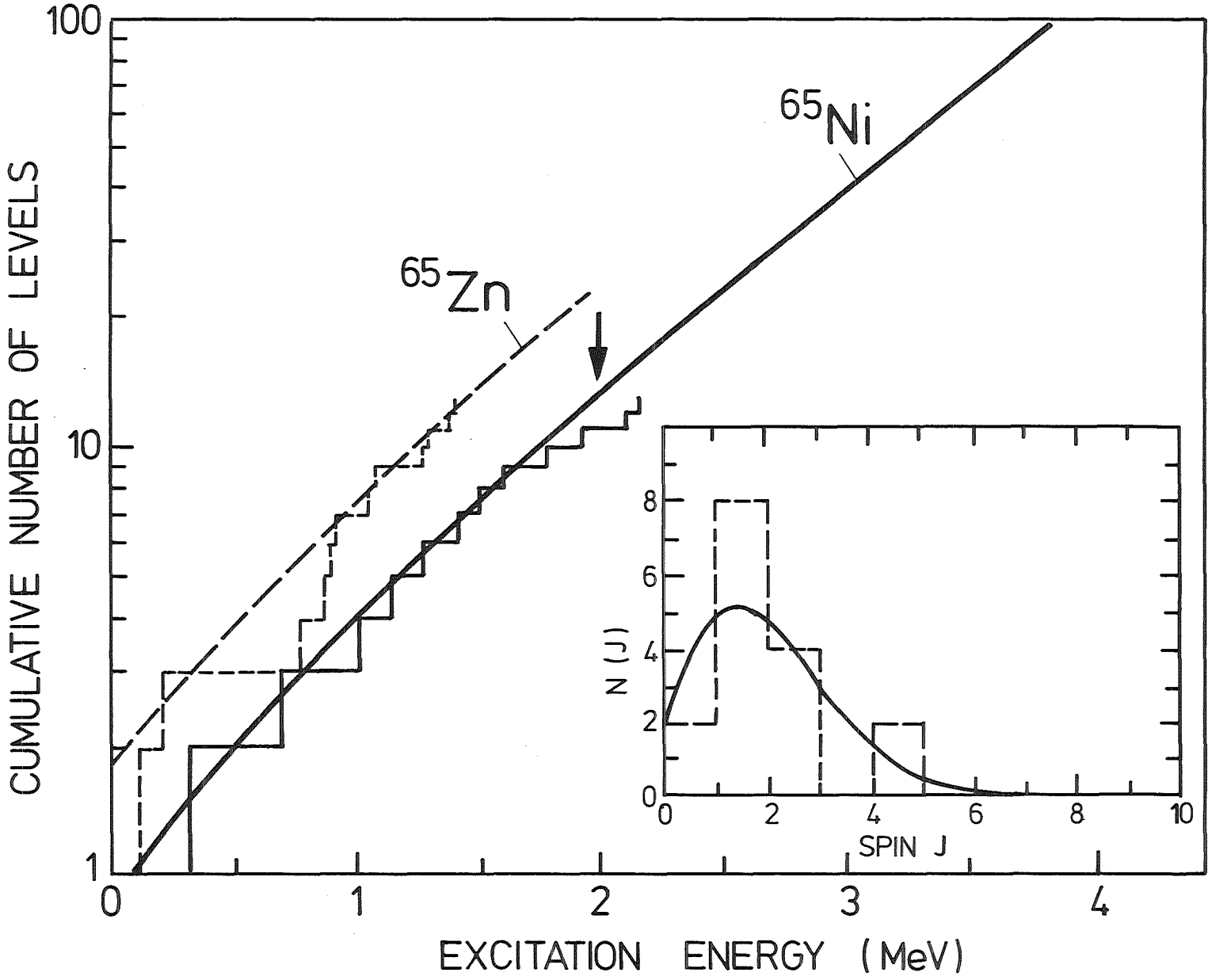
100
10
1
CUMULATIVE NUMBER OF LEVELS
65Ni
65Zn
0
1
2
3
4
EXCITATION ENERGY (MeV)
N (J)
8
6
4
2
0
0
2
4
6
8
10
SPIN J

Fig. 5

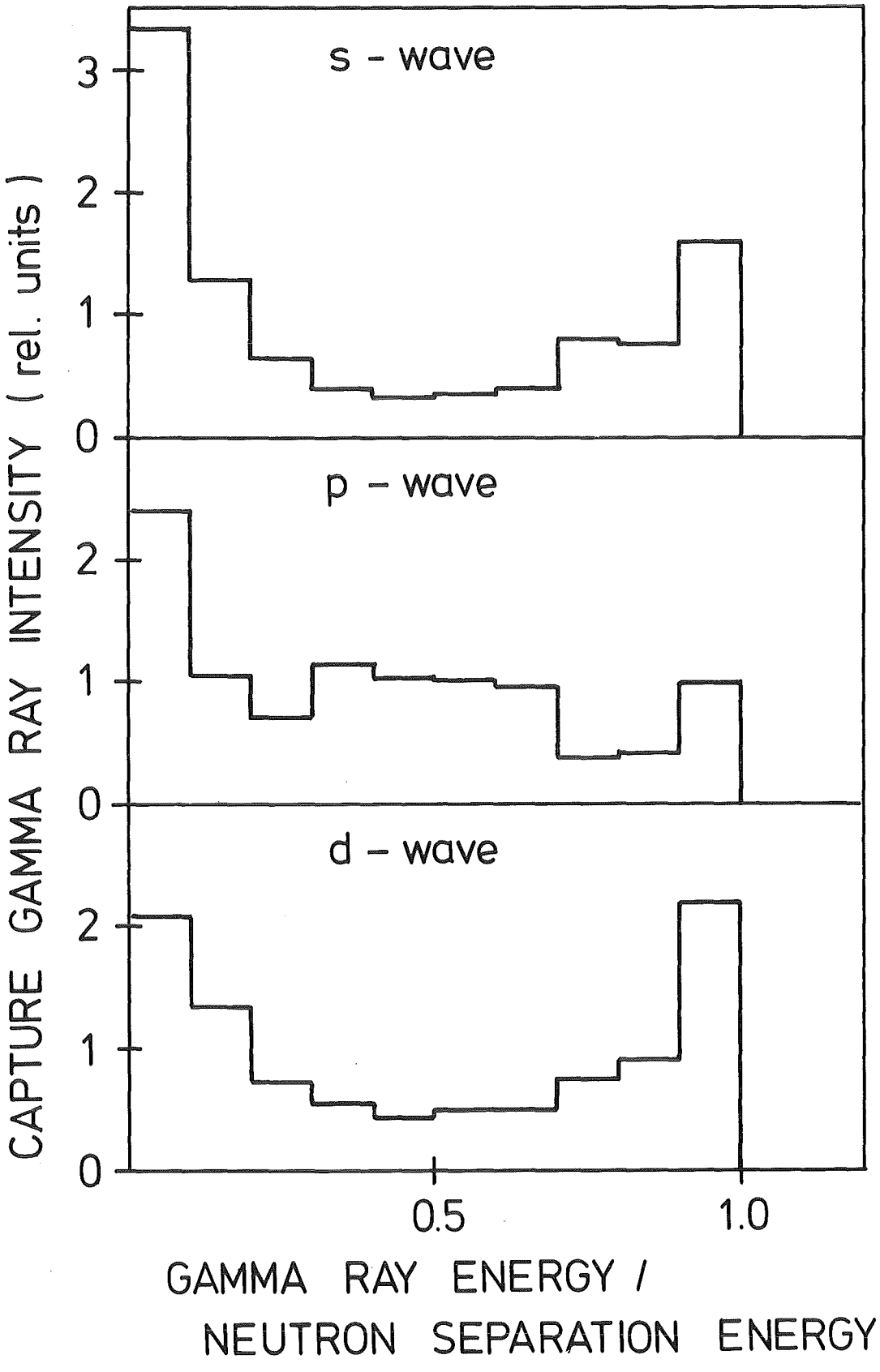
s - wave
p - wave
d - wave
CAPTURE GAMMA RAY INTENSITY (rel. units)
0
1
2
3
0.5
1.0
GAMMA RAY ENERGY /
NEUTRON SEPARATION ENERGY

Fig. 6